

Entanglement Entropy and Wilson Loop in Stückelberg Holographic Insulator/Superconductor Model

Rong-Gen Cai*, Song He†, Li Li‡, Li-Fang Li§

State Key Laboratory of Theoretical Physics,
Institute of Theoretical Physics, Chinese Academy of Sciences,
P.O. Box 2735, Beijing 100190, China

September 05, 2012

Abstract

We study the behaviors of entanglement entropy and vacuum expectation value of Wilson loop in the Stückelberg holographic insulator/superconductor model. This model has rich phase structures depending on model parameters. Both the entanglement entropy for a strip geometry and the heavy quark potential from the Wilson loop show that there exists a “confinement/deconfinement” phase transition. In addition, we find that the non-monotonic behavior of the entanglement entropy with respect to chemical potential is universal in this model. The pseudo potential from the spatial Wilson loop also has a similar non-monotonic behavior. It turns out that the entanglement entropy and Wilson loop are good probes to study the properties of the holographic superconductor phase transition.

Contents

1	Introduction	2
2	Stückelberg Insulator/Superconductor Model	4

*E-mail: cairg@itp.ac.cn

†E-mail: hesong@itp.ac.cn

‡E-mail: liliphy@itp.ac.cn

§E-mail: lilf@itp.ac.cn

3	Thermodynamics and Phase Transition	5
4	Entanglement Entropy	7
5	Wilson Loop	11
5.1	Temporal Wilson Loop	12
5.2	Spatial Wilson Loop	16
6	Conclusion and Discussions	18

1 Introduction

The entanglement entropy is expected to be a key quantity to understand some properties in quantum field theories and in many-body physics (see, for example, Refs. [1, 2]). For a given system, the entanglement entropy of one subsystem with its complement is defined as the von Neumann entropy. The entanglement entropy of the subsystem measures how the subsystem and its complement are correlated each other. As a von Neumann entropy, the entanglement entropy is also directly related to the degrees of freedom of the system. In addition, in quantum many-body physics, the entanglement entropy is a good quantity to characterize different phases and associated phase transitions. However, the calculation of entanglement entropy is very difficult except for the case in 1 + 1 dimensions. In the spirit of the AdS/CFT correspondence [3, 4, 5, 6], a holographic proposal to calculate the entanglement entropy for strongly coupled field theories has been presented in Ref. [7] (for reviews see [8, 9]).

On the other hand, while various aspects of holographic superconductor models have been intensively studied (see, for example, Refs. [10, 11, 12, 13, 14, 15, 16, 17, 18, 19, 20, 21, 22, 23, 24, 25, 26, 27, 28, 29, 30, 31]), the study of entanglement entropy in the holographic superconducting phase transition is just initialed. Refs. [32, 33] studied the behaviors of entanglement entropy for a strip geometry in the holographic s-wave and p-wave conductor/superconductor models. It turns out that the entanglement entropy is a good probe to investigate the holographic phase transition, the entanglement entropy behaves like the thermal entropy of background black holes, it can indicate not only the appearance, but also the order of the phase transition. In a recent paper [34], the authors investigated the behavior of the entanglement entropy for a strip geometry in a simple holographic insulator/superconductor model at zero temperature. In this model, the phase transition is a second order one. It was found that the entanglement entropy as a function of chemical potential is not monotonic in the superconducting phase. The entanglement entropy at first increases and reaches its maximum at a certain chemical potential and then decreases monotonically as chemical potential increases. The non-monotonic behavior of entanglement entropy in the superconducting phase looks strange. Due to the lack of details of dual field theory, we did not give a convinced interpretation, although some possible causes on this behavior were discussed there [34].

In the holographic insulator/superconductor model [35], the normal insulator phase is described by a pure AdS soliton solution. As one increases the chemical potential, the pure AdS soliton background will become unstable to develop some kind of scalar “hair”. The emergence of scalar “hair” induces the symmetry breaking and gives a finite vacuum expectation value of the dual operator in the field theory side. The soliton solution with scalar “hair” describes a superconducting phase. The scalar “hair” therefore plays the role of the order parameter in the holographic phase transition.

In this paper we are going to further study the behavior of the entanglement entropy in the holographic insulator/superconductor phase transition by generalizing the discussion to the case in the Stückelberg holographic insulator/superconductor model [36]. The aim is two-fold. On the one hand, we would like to see whether the non-monotonic behavior is universal or not. On the other hand, the phase structure is rather rich in the Stückelberg holographic insulator/superconductor model. As we will see shortly, depending on the model parameters, the superconducting phase transition could be second order or first order, and further a first order phase transition also occurs in the superconducting phase.

The Stückelberg holographic insulator/superconductor model is labeled by two parameters. One is β determining the strength of the back reaction. The other is ζ determining the form of interaction between the scalar field and Maxwell field. Both of them can change the order of the phase transition. As ζ is vanishing, an equivalent model has been studied in Ref. [37]. It shows that as one increases the strength of the back reaction, the order of the phase transition is changed from second order to first order. For the intermediate strength of the back reaction, although the insulator/superconductor transition is second order, a new phase transition emerges in superconducting phase. We fix the strength of the back reaction and study the effect with the change of ζ . Interestingly, the resulting phenomenon is qualitatively similar to the above case. The order of the phase transition is second order for small ζ and first order for large ζ . For the intermediate value of ζ , the phase transition is second order, however, the grand potential in superconducting phase develops a “swallow tail” indicating a new phase transition.

We calculate the entanglement entropy for a strip geometry in this model, and find that the entanglement entropy can indicate not only the appearance of phase transition, but also the order of the phase transition. Further, no matter the order of the phase transition, the entanglement entropy versus chemical potential is always non-monotonic in the superconducting phase. More precisely, at the beginning of the transition, the entropy increases and reaches its maximum at a certain chemical potential and then decreases monotonically. It indicates that the non-monotonic behavior of entanglement entropy as a function of chemical potential is universal in the holographic s-wave insulator/superconductor model.

Apart from the entanglement entropy, there is another nonlocal quantity, Wilson loop, which can describe some properties of gauge field theories. In the AdS/CFT correspondence, the vacuum expectation value (VEV) of Wilson loop can also be calculated holographically. In order to give further insights into the holographic insulator/superconductor phase transition, we study the behaviors of temporal Wilson loop and spatial Wilson loop across the holographic phase transition. From the VEV of Wilson loops, we extract the heavy quark potential which describes the interaction strength between quark and anti-

quark. From the entanglement entropy and the heavy quark potential, it shows that there exists a “confinement/deconfinement” phase transition in the dual field theory describing the insulator/superconductor model. In addition, different from the phenomenon observed in the entanglement entropy, the (pseudo) heavy quark potential versus chemical potential in the superconducting phase will show the monotonic behavior or non-monotonic behavior, depending on the model parameters.

This paper is organized as follows. In section (2), we introduce the Stückelberg holographic model. In section (3), the insulator/superconductor phase transition and its thermodynamics are investigated in detail. Section (4) is devoted to investigating the behavior of entanglement entropy in the holographic model. In section(5), we study the behavior of temporal Wilson loop and spatial Wilson loop with respect to chemical potential and distance between quark and antiquark. The conclusion and some discussions are included in section (6).

2 Stückelberg Insulator/Superconductor Model

The Stückelberg holographic superconductor model which contains a real scalar field ψ , a real pseudoscalar field p and a Maxwell gauge field reads [36, 38, 39]

$$S = \int d^5x \sqrt{-g} \left[\frac{1}{2\kappa^2} (\mathcal{R} + \frac{12}{L^2}) + \frac{1}{\tilde{g}^2} L_{matter} \right], \quad (1)$$

$$L_{matter} = -\frac{1}{4} F_{\mu\nu} F^{\mu\nu} - \nabla_\mu \psi \nabla^\mu \psi - m^2 \psi^2 - |\mathcal{F}(\psi)| (\nabla_\mu p - A_\mu) (\nabla^\mu p - A^\mu),$$

where κ is the gravitational constant and \mathcal{F} is a function of ψ . In this paper we consider a simple case $\mathcal{F}(\psi) = \psi^2 + \zeta \psi^6$, where ζ is a model parameter determining the interaction form and is assumed to be non-negative to ensure the positivity of the kinetic term for p . For other forms of \mathcal{F} , see [36, 38, 39]. The local $U(1)$ gauge symmetry in this theory is given by

$$p \rightarrow p + \theta(x^\mu), \quad A_\mu \rightarrow A_\mu + \nabla_\mu \theta(x^\mu). \quad (2)$$

We use this symmetry to set $p = 0$ from now on. Here we define a parameter $\beta \equiv \kappa/\tilde{g}$ which measures the strength of the back reaction of the matter fields on the background geometry.

The equations of motion coming from the above action are

$$\mathcal{R}_{\mu\nu} - \frac{\mathcal{R}}{2} g_{\mu\nu} - \frac{6}{L^2} g_{\mu\nu} = \beta^2 [F_{\mu\lambda} F_\nu{}^\lambda + 2\nabla_\mu \psi \nabla_\nu \psi + 2(\psi^2 + \zeta \psi^6) A_\mu A_\nu + g_{\mu\nu} L_{matter}],$$

$$\nabla_\mu \nabla^\mu \psi - m^2 \psi = (\psi + 3\zeta \psi^5) A_\mu A^\mu, \quad (3)$$

$$\nabla_\nu F^{\nu\mu} = 2(\psi^2 + \zeta \psi^6) A^\mu.$$

Our ansatz for the metric and matter fields are given by

$$ds^2 = \frac{L^2}{r^2} \frac{dr^2}{g(r)} + r^2 (-f(r) dt^2 + dx^2 + dy^2 + g(r) e^{-\chi(r)} d\eta^2), \quad (4)$$

$$\psi = \psi(r), \quad A = \phi(r)dt, \quad (5)$$

where $g(r)$ vanishes at the tip of the soliton $r = r_0$. Further, in order to avoid a conical singularity at the tip r_0 , η should be made with an identification

$$\eta \sim \eta + \Gamma, \quad \Gamma = \frac{4\pi L e^{\frac{\chi(r_0)}{2}}}{r_0^2 g'(r_0)}. \quad (6)$$

The independent equations of motion in terms of the above ansatz are deduced as follows.

$$\begin{aligned} \psi'' + \left(\frac{5}{r} + \frac{f'}{2f} + \frac{g'}{g} - \frac{\chi'}{2}\right)\psi' + \frac{L^2\phi^2}{r^4fg}(\psi + 3\zeta\psi^5) - \frac{L^2m^2}{r^2g}\psi &= 0, \\ \phi'' + \left(\frac{3}{r} - \frac{f'}{2f} + \frac{g'}{g} - \frac{\chi'}{2}\right)\phi' - \frac{2L^2\phi}{r^2g}(\psi^2 + \zeta\psi^6) &= 0, \\ f'' + \left(\frac{2}{r} - \frac{f'}{2f} + \frac{\chi'}{2}\right)f' + \left(\frac{3\chi'}{r} + 4\beta^2\psi'^2\right)f - \frac{2\beta^2\phi'^2}{r^2} &= 0, \\ \left(\frac{3}{r} - \frac{f'}{2f}\right)g' + \left(\frac{12}{r^2} + \frac{f'\chi'}{2f} + 2\beta^2\psi'^2 + \frac{\beta^2\phi'^2}{r^2f}\right)g + \frac{2L^2\beta^2\phi^2}{r^4f}(\psi^2 + \zeta\psi^6) + \frac{2L^2\beta^2m^2\psi^2 - 12}{r^2} &= 0, \\ \left(\frac{3f}{r} + f'\right)\chi' - \left(\frac{3}{r} + \frac{g'}{g}\right)f' + \frac{4L^2\beta^2\phi^2}{r^4g}(\psi^2 + \zeta\psi^6) + 4\beta^2f\psi'^2 &= 0. \end{aligned} \quad (7)$$

In our numerical calculations, we choose $m^2L^2 = -\frac{15}{4}$ and work in units with $L = 1$. However, this analysis can be generalized to any mass case above the Breitenloher-Freedman bound $m^2L^2 > -4$. In order to match the asymptotical AdS boundary, the matter and metric fields near the boundary $r \rightarrow \infty$ should have the form

$$\begin{aligned} \psi &= \frac{\psi_0}{r^{3/2}} + \frac{\psi_1}{r^{5/2}} + \dots, \quad \phi = \phi_0 - \frac{\phi_2}{r^2}, \\ f &= 1 + \frac{f_4}{r^4} + \dots, \quad g = 1 + \frac{g_4}{r^4} + \dots, \quad \chi = \frac{\chi_4}{r^4} + \dots, \end{aligned} \quad (8)$$

where $\psi_0, \psi_1, \phi_0, \phi_2, f_4, g_4$ and χ_4 are all constants. It is well-known that in five-dimensional AdS space-time, when $-4 < m^2L^2 < -3$, the scalar field admits two different quantizations related by a Legendre transformation. ψ_0 can either be identified as a source or an expectation value. In this paper we consider it as source and set $\psi_0 = 0$ to accomplish spontaneous symmetry breaking. The quantities ϕ_0, ϕ_2 and ψ_1 are related to the chemical potential μ , charge density ρ and the vacuum expectation value of the scalar operator \mathcal{O} which has scaling dimension $\Delta = \frac{5}{2}$ in the dual field theory on the boundary, i.e., $\mu = \phi_0, \rho = \frac{2\beta^2}{\kappa^2L}\phi_2$ and $\langle \mathcal{O} \rangle = \frac{2\beta^2(2\Delta-4)}{\kappa^2L}\psi_1 = \frac{2\beta^2}{\kappa^2L}\psi_1$.

3 Thermodynamics and Phase Transition

In gauge/gravity duality the grand potential (Gibbs free energy) Ω of the boundary thermal state is identified with temperature times the on-shell bulk Euclidean action. Namely

$\Omega = TS_{Euclidean}$. The Euclidean action must include the Gibbons-Hawking boundary term for a well-defined Dirichlet variational principle and further a surface counter term for removing divergence

$$S_{Euclidean} = - \int d^5x \sqrt{g} \left[\frac{1}{2\kappa^2} \left(\mathcal{R} + \frac{12}{L^2} \right) + \frac{1}{\tilde{g}^2} L_{matter} \right] - \frac{1}{\kappa^2} \int_{r \rightarrow \infty} d^4x \sqrt{h} \mathcal{K} + S_{ct}, \quad (9)$$

where h is the induced metric on the boundary $r \rightarrow \infty$, and \mathcal{K} is the trace of the extrinsic curvature. S_{ct} is the counter term given by

$$S_{ct} = \frac{1}{\kappa^2} \int_{r \rightarrow \infty} d^4x \sqrt{h} \left(\frac{3}{L} + \beta^2 \frac{4 - \Delta}{L} \psi^2 \right). \quad (10)$$

For our soliton solution (4), there is no horizon and associated Hawking temperature and thermal entropy vanishes. But for the Euclidean sector of the solution (4), one can introduce an arbitrary inverse temperature ($1/T$) as the period of the Euclidean time coordinate. Due to the fact that the soliton solution is static, the integration over the Euclidean time in the Euclidean action gives an inverse temperature factor $1/T$, which just cancels the temperature factor in the grand potential and leads a finite grand potential. Using the on-shell condition and the expansion of matter and metric functions at infinity $r \rightarrow \infty$, the grand potential Ω is found to be given as

$$\frac{2L\kappa^2\Omega}{V_3} = g_4, \quad (11)$$

with $V_3 = \int dx dy d\eta$. Since we have scaled Γ to be πL , one has $g_4 = -1$ in the normal insulator phase.

Figure (1) shows the behavior of the condensate with respect to chemical potential for the back reaction parameter $\beta = 0.25$ ¹. When ζ is small, we see from Figure (1) that as the chemical potential μ exceeds a critical value μ_c the condensate emerges, which implies a superconducting phase appears. On the other hand, when $\mu < \mu_c$, the scalar hair vanishes. This is identified as the insulator phase, since the system has a mass gap $\sim 1/\Gamma$. The insulator/superconductor phase transition here is typically second order and in this case, the critical chemical potential μ_c does not depend on ζ , the critical chemical potential is given by $\mu_c \simeq 1.888$ ².

As we increase ζ to $\zeta \simeq 0.5$, an additional complication appears. The condensate versus chemical potential does not have a monotonic behavior (see the red curve in Figure (1)). As we can see clearly in the left plot of Figure (2), the grand potential with respect to chemical potential develops a ‘‘swallow tail’’, which is a typical signal for a first order phase transition. It implies that there is a new phase transition within the superconducting phase. If we continue to increase ζ , the insulator/superconductor phase transition will

¹In our numerical calculations of this paper we always take $\beta = 0.25$ and show rich phase structure by changing the parameter ζ .

²When ζ is beyond a certain value, the superconducting phase transition will become a first order one. In that case, the critical chemical will depend on ζ .

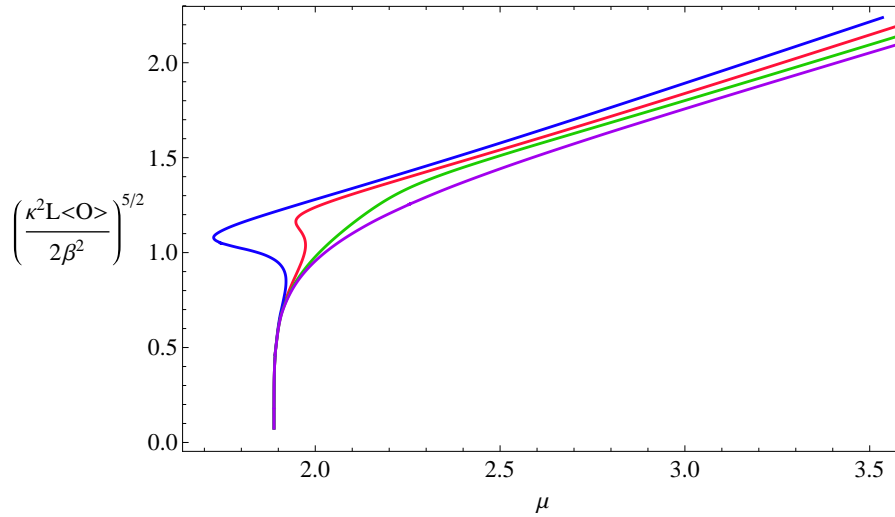


Figure 1: The condensate of operator \mathcal{O} versus chemical potential μ for $\beta = 0.25$. Lines from right to left are for $\zeta = 0$ (purple), $\zeta = 0.2$ (green), $\zeta = 0.65$ (red) and $\zeta = 1.6$ (blue), respectively. Γ is scaled to be πL .

become first order when $\zeta > 1$, which can be seen in the right plot of Figure (2).³ This is qualitatively similar to the case in Ref. [37] where the effect of back reaction on the insulator/superconductor was studied in the case with vanishing ζ . The condensate becomes larger with the increase of ζ , which means that the scalar hair will be more difficult to be formed in the AdS soliton background with larger ζ .

4 Entanglement Entropy

Now let us begin to study the behavior of entanglement entropy in this holographic superconductor model. The holographic method to calculate entanglement entropy is as follows. Consider a strongly coupled field theory with gravity dual, the entanglement entropy of subsystem \mathcal{A} with its complement is given by searching for the minimal area surface $\gamma_{\mathcal{A}}$ extended into the bulk with the same boundary $\partial\mathcal{A}$ of \mathcal{A} . Then the entanglement entropy of \mathcal{A} with its complement is given by the “area law” [7]

$$S_{\mathcal{A}} = \frac{2\pi}{\kappa^2} \text{Area}(\gamma_{\mathcal{A}}), \quad (12)$$

where κ is the gravitational constant.

We consider the subsystem \mathcal{A} with a straight strip geometry with a finite width ℓ along the x direction, along the η direction with a period Γ , but infinitely extending along the y

³It is worth pointing out here that if the back reaction parameter β is larger enough, the transition will always be first order, no matter how small the value of ζ is chosen. However, we do not consider the case in this paper.

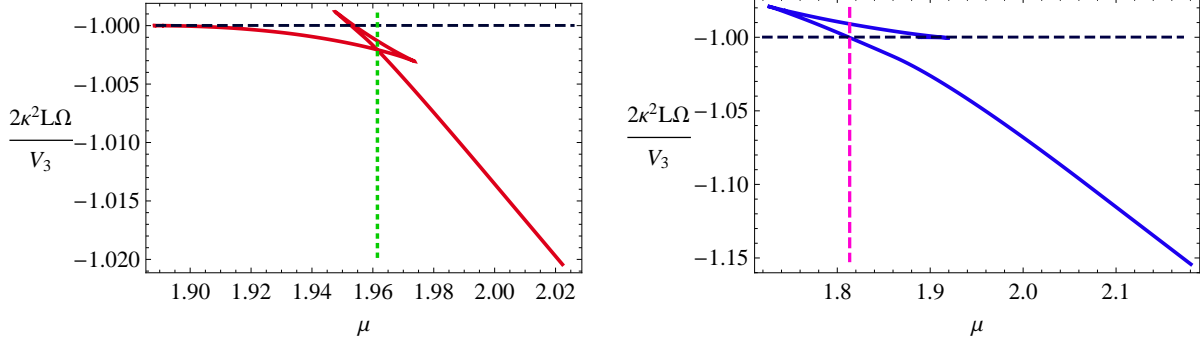


Figure 2: The grand potentials of the soliton with scalar hair (solid) and the soliton without scalar hair (dashed black) with respect to chemical potential for $\zeta = 0.65$ (left plot) and $\zeta = 1.6$ (right plot), respectively. Γ is scaled to be πL and $\beta = 0.25$. The left plot has a second order phase transition at $\mu \simeq 1.888$, but a discontinuity at $\mu_0 \simeq 1.962$ (denoted by dotted vertical green line) in superconducting phase. The right plot shows the typical first order phase transition and the critical chemical potential denoted by vertical dashed pink line is $\mu_c \simeq 1.813$.

direction. The subsystem \mathcal{A} sites on the slice $r = \frac{1}{\epsilon}$, where $\epsilon \rightarrow 0$ is the UV cutoff. The holographic dual surface $\gamma_{\mathcal{A}}$ is defined as a three-dimensional surface

$$t = 0, \quad r = r(x), \quad -\frac{R}{2} < y < \frac{R}{2} \quad (R \rightarrow \infty), \quad 0 \leq \eta \leq \Gamma. \quad (13)$$

We are first interested in the case that the surface is smooth. The holographic surface $\gamma_{\mathcal{A}}$ starts from $x = \frac{\ell}{2}$ at $r = \frac{1}{\epsilon}$, extends into the bulk until it reaches $r = r_*$, then returns back to the AdS boundary $r = \frac{1}{\epsilon}$ at $x = -\frac{\ell}{2}$. In this case, the entanglement entropy is given by

$$S_{\mathcal{A}}^{connect} = \frac{4\pi L}{\kappa^2} R \Gamma \int_{r_*}^{\frac{1}{\epsilon}} \frac{r^4 \sqrt{g(r)} e^{-\chi(r)}}{\sqrt{r^6 g(r) e^{-\chi(r)} - r_*^6 g(r_*) e^{-\chi(r_*)}}} dr = \frac{2\pi L}{\kappa^2} R \Gamma \left(\frac{1}{\epsilon^2} + S^{con} \right), \quad (14)$$

where the UV cutoff $1/\epsilon$ has been taken into consideration. The width ℓ of the subsystem \mathcal{A} and r_* are related by

$$\frac{\ell}{2} = \int_{r_*}^{\frac{1}{\epsilon}} \frac{L}{r^2 \sqrt{g(r) \left(\frac{r^6 g(r) e^{-\chi(r)}}{r_*^6 g(r_*) e^{-\chi(r_*)}} - 1 \right)}} dr. \quad (15)$$

In fact, there are two solutions for the connected configuration. See Figure (3). In addition, there is also a disconnected configuration describing two separated surfaces located at $x = \pm \frac{\ell}{2}$ respectively and extending to the bulk and reaching at the tip of the soliton geometry. The entropy for this disconnected geometry is independent of ℓ , and given by

$$S_{\mathcal{A}}^{disconnect} = \frac{4\pi L}{\kappa^2} R \Gamma \int_{r_0}^{\frac{1}{\epsilon}} r e^{-\frac{\chi(r)}{2}} dr = \frac{2\pi L}{\kappa^2} R \Gamma \left(\frac{1}{\epsilon^2} + S^{discon} \right). \quad (16)$$

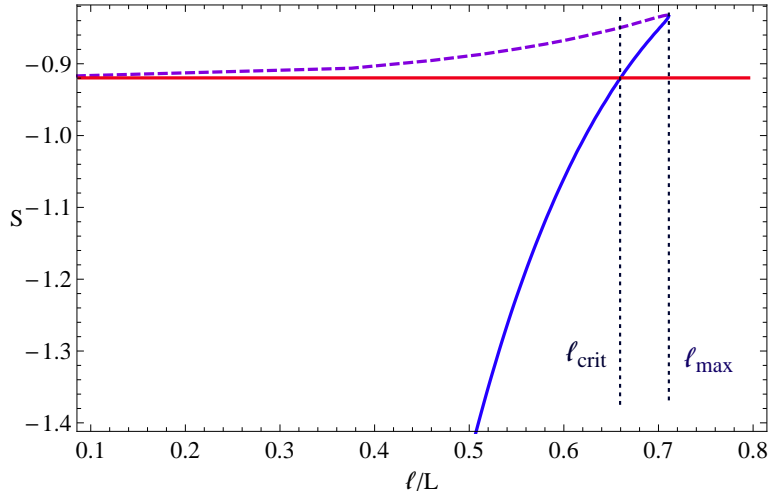


Figure 3: The entanglement entropy as a function of strip width ℓ for $\beta = 0.25$, $\zeta = 0.65$ and $\mu \simeq 2.276$. The dashed purple and solid blue curves come from the connected configuration, while the solid red one comes from the disconnected configuration. The lowest curve is physically favored compared with others. In this figure $\ell_{crit} \simeq 0.66L$ and $\ell_{max} \simeq 0.71L$.

We find that the entanglement entropy with respect to strip width ℓ behaves quite similar for different choice of parameters, i.e., β , ζ and μ . We draw Figure (3) with $\beta = 0.25$, $\zeta = 0.65$ and $\mu \simeq 2.276$ as a concrete example. The connected configuration does not exist when $\ell > \ell_{max}$. The physical solution comes from the trivial disconnected geometry and the entropy is independent of strip width. On the contrary, there are three different branches when $\ell < \ell_{max}$, i.e., the upper branch (dashed purple), the lower branch (solid blue) and the middle branch (solid red). The first two curves correspond to the connected surface, while the third curve comes from the disconnected one. We trace over the physical entropy by always choosing the lowest branch. As we can see from Figure (3), the lower branch (solid blue) is finally favored as we decrease ℓ . Hence, there is a critical value ℓ_{crit} below which the lower branch is physically favored. Thus, as we change ℓ , a phase transition occurs at ℓ_{crit} , which is just the so called “confinement/deconfinement” phase transition [40, 41, 42]. To be precise, for $\ell < \ell_{crit}$, the entanglement entropy comes from the connected surface and exhibits non-trivial dependence on ℓ , which describes a “deconfinement” phase. For $\ell > \ell_{crit}$, the entropy is dominated by the disconnected configuration and is ℓ independent, which indicates a “confinement” phase.

To summarize, there are totally four “phases” in the dual boundary field theory, i.e., the insulator phase, superconductor phase, and their corresponding confinement/deconfinement phases. These phases are characterized by the chemical potential μ and strip width ℓ . In particular, the strip width controls the “confinement/deconfinement” phase transition⁴.

⁴Strictly speaking, the term phase transition here is inappropriate since the system itself, i.e., the state of the boundary field theory, does not change at all as one changes ℓ . However, this observed behavior here is quite similar to the one in the thermodynamic confinement/deconfinement phase transitions and therefore we follow Refs. [40, 41, 42] and adopt the terminology “phase transition” to describe this behavior.

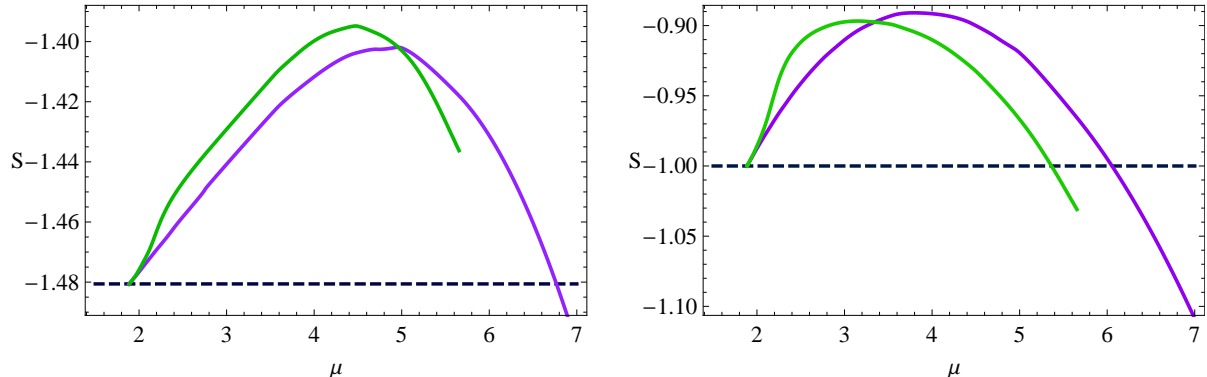


Figure 4: The entanglement entropy as a function of chemical potential for $\zeta = 0$ (purple curves) and $\zeta = 0.2$ (green curves) at fixed $\ell/L = 0.5$ (within “deconfining phase”, left plot) and $\ell/L \rightarrow \infty$ (within “confining phase”, right plot), respectively. The transition from insulator to superconductor is second order here. In both two plots, the solid curves come from superconducting phase, while the dashed black lines come from insulator phase.

It is instructive to study how the entanglement entropy changes with chemical potential by fixing strip width ℓ . We first focus on the second order phase transition case, which is presented in Figure (4). We can see that, at the beginning of the phase transition, the entanglement entropy increases continuously with chemical potential both in “deconfinement phase” and “confinement phase” and reaches its maximum at a certain chemical potential μ_{max} , then it decrease monotonically. Furthermore, the entanglement entropy is continuous at critical chemical potential μ_c , but its slop has a discontinuous change at μ_c . The behavior of the entanglement entropy across the phase transition point indicates that the transition is a second order one.

When $0.5 < \zeta < 1$, a jump in the condensate (the red curve in Figure (1)) and a “swallow tail” in the grand potential (see the left plot in Figure (2)) appear, although the phase transition is still a second order one at μ_c . Interestingly, we can also see a jump in Figure (5) which shows the entanglement entropy as a function of chemical potential at fixed strip width. Tracing the physical curve, we find that the entropy increases at the beginning of the transition, then there is a sudden jump at the chemical potential $\mu_0 \simeq 1.962$. The sudden jump of entropy indicates a first order phase transition there.

For sufficiently large ζ , the insulator/superconductor transition becomes first order. The entanglement entropy with respect to chemical potential is presented in Figure (6). Comparing with Figure (4) and (5), we can see a dramatic change in the first order case. Although the entropy in superconducting phase also behaves non-monotonically with respect to μ , the entropy as well as its slop at the critical point have a discontinuous jump. Once again, it is a signal of a first order transition.

In Figure (7), we plot the critical length ℓ_{crit} of the “confinement/deconfinement” phase transition with respect to the chemical potential in the superconducting phase. For small ζ , ℓ_{crit} first increases and form a peak, then it will increase continuously for large chemical

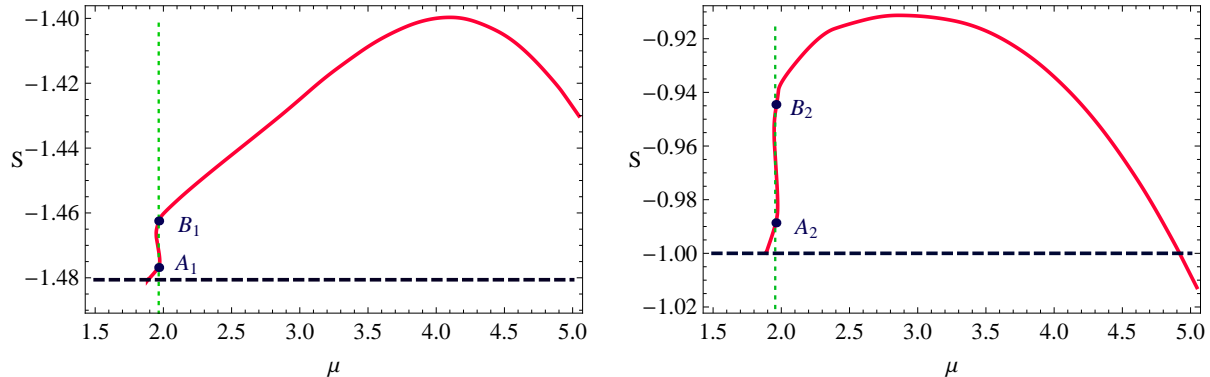


Figure 5: The entanglement entropy as a function of chemical potential for $\zeta = 0.65$ at fixed $\ell/L = 0.5$ (within “deconfinement phase”, left plot) and $\ell/L \rightarrow \infty$ (within “confinement phase”, right plot), respectively. The transition from insulator to superconductor is second order, but a discontinuity at $\mu_0 \simeq 1.962$ (denoted by dotted vertical line) within the superconducting phase. In both two plots, the solid red curves are from superconducting phase, while the dashed black lines are from insulator phase. Trace the physical curve by choosing the dashed black line for $\mu < \mu_c$, then choosing the red curve which has a jump from point A to point B at $\mu_0 \simeq 1.962$.

potential. As we increase ζ , the position of the peak moves toward to the region with small chemical potential and will be finally cut off since the transition is first order for large ζ , as we can see that the dotted part of the blue curve in Figure (7) is not thermodynamically favored. Here an remarkable point is that the critical length as a function of the chemical potential is not monotonic. This is of course related to the fact that the entanglement entropy is not a monotonic function of the chemical potential.

We can see from Figures (4), (5) and (6) that although the phase structures are different in three cases, the entanglement entropy with respect to chemical potential are always non-monotonic in superconducting phase. The discontinuity or jump at critical point indicates some kind of significant reorganization of the degrees of freedom of the system, since new degrees of freedom are expected to emerge in new phase. The non-monotonic behavior of the entanglement entropy is interesting. To further study its implication, in the next section, we will discuss the behavior of another non-local quantity, Wilson loop, in the superconducting phase.

5 Wilson Loop

From the VEV of Wilson loop one can extract the interaction potential between a quark-antiquark pair in gauge field theory. Therefore the VEV of Wilson loop is thought of as a proper quantity to describe the confinement/deconfinement phase transition of gauge field theory. In the AdS/CFT correspondence, a proposal for the VEV of Wilson loop is presented in Refs. [43, 44, 45]. In this section, following the proposal we will discuss the

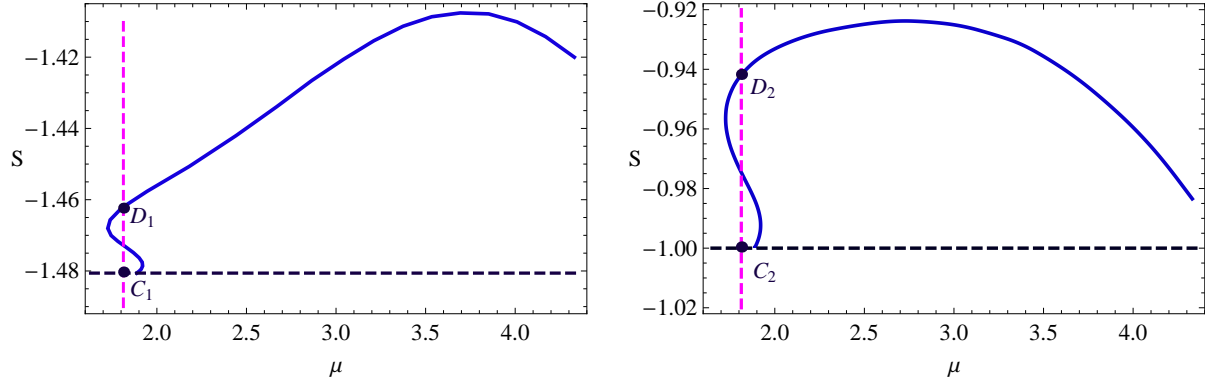


Figure 6: The entanglement entropy as a function of chemical potential for $\zeta = 1.6$ at fixed $\ell/L = 0.5$ (within “deconfinement phase”, left plot) and $\ell/L \rightarrow \infty$ (within “confinement phase”, right plot), respectively. The transition is first order and the critical chemical potential denoted by vertical dashed pink line is $\mu_c \simeq 1.813$. In both two plots, the solid blue curves are from superconducting phase, while the dashed black lines are from insulator phase. Trace the physical curve by choosing the dashed black line for $\mu < \mu_c$, and for $\mu > \mu_c$, choosing the blue curve starting from point D.

behavior of the VEV of Wilson loop in the holographic insulator/superconductor phase transition. We will consider two kinds of Wilson loop: One is a temporal Wilson loop; the other is a spatial Wilson loop. In both cases, we will show the behavior of the interaction potential with respect to the distance ℓ between quark and antiquark and to the background chemical potential μ .

5.1 Temporal Wilson Loop

In $SU(N)$ gauge theory, the interaction potential for heavy quark-antiquark ($Q\bar{Q}$) pair can be calculated from the Wilson loop

$$W[C] = \frac{1}{N} \text{Tr} P \exp[i \oint_C A_\mu dx^\mu], \quad (17)$$

where A_μ is the gauge field, the trace is over the fundamental representation, P stands for path ordering. C denotes a closed loop in space-time, which is a rectangle with one direction along the temporal direction of length T and the other spatial direction of length ℓ . The Wilson loop describes the creation of a $Q\bar{Q}$ pair with distance ℓ at some time $t_0 = 0$ and the annihilation of this pair at time $t = T$. For $T \rightarrow \infty$, the VEV of the Wilson loop goes as $\langle W(C) \rangle \propto e^{-TV_{Q\bar{Q}}}$. In terms of the AdS/CFT dictionary, the VEV of the Wilson loop in four dimensions should be equal to the string partition function on the curved space, with the string world sheet ending on the contour C at the boundary of the curved space [43]

$$\langle W^{4d}[C] \rangle = Z_{string}^{5d}[C] \simeq e^{-S_{x-t}[C]}, \quad (18)$$

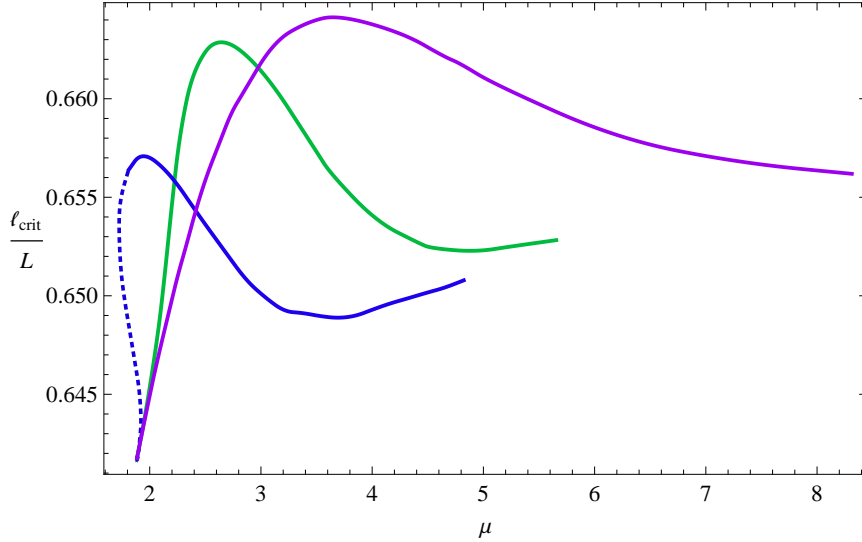


Figure 7: The critical length as a function of chemical potential in superconducting phase, where the purple curve (up) is for $\zeta = 0$, the green curve (middle) is for $\zeta = 0.2$ and the blue curve (down) is for $\zeta = 1.6$. The dotted part of the line for $\zeta = 1.6$ (blue) is not thermodynamically favored, trace the physical curve by always choosing the solid line. Note that the curve for $\zeta = 0$ (purple) will continue to increase large chemical potential as other curves.

where S_{x-t} is the classical world sheet action of the Nambu-Goto form

$$S_{x-t} = \frac{1}{2\pi\alpha'} \int d\tau d\sigma \sqrt{\text{Det}\chi_{ab}}, \quad (19)$$

and α' is the string tension with dimension $[\text{energy}]^{-2}$, and χ_{ab} is the induced world sheet metric with a, b the indices in the $(\tau = t, \sigma = x)$ coordinates on the world sheet. In this subsection, we follow the standard procedure [43, 44, 45] to extract the static heavy quark potential $V_{Q\bar{Q}}$ in the general metric background (4). To do this, as in Ref. [46], we should consider two kinds of string configurations: one is a connected configuration and the other is a disconnected one.

For the connected configuration, the string starts at the AdS boundary $r = 1/\epsilon$ and $x = \ell/2$, goes into the bulk, turns around at $r = r_*$ and $x = 0$, and finally reaches at $r = 1/\epsilon$ and $x = -\ell/2$. For the disconnected configuration, two straight strings start at $r = 1/\epsilon$ with $x = \pm\ell/2$, respectively and end at the tip of the background soliton, $r = r_0$. Here $1/\epsilon$ is the UV cutoff and ℓ is the distance between two quarks.

We now take the gauge $t = \tau$ and $x(r) = \sigma$. Then the induced metric χ_{ab} can be expressed as

$$ds^2 = \chi_{ab} dx^a dx^b = g_{\mu\nu} \frac{dx^\mu}{dx^a} \frac{dx^\nu}{dx^b} dx^a dx^b = \left[\frac{L^2}{r^2 g(r)} \left(\frac{dr}{d\sigma} \right)^2 + r^2 \right] d\sigma^2 - r^2 f(r) d\tau^2. \quad (20)$$

Thus, we need to minimize the following Nambu-Goto action functional

$$S_{x-t}^{con}[r] = \frac{1}{2\pi\alpha'} \int_0^T \int_{-\frac{\ell}{2}}^{\frac{\ell}{2}} d\tau d\sigma \sqrt{\left(\frac{L^2}{r^2 g(r)} \left(\frac{dr}{d\sigma}\right)^2 + r^2\right) r^2 f(r)}. \quad (21)$$

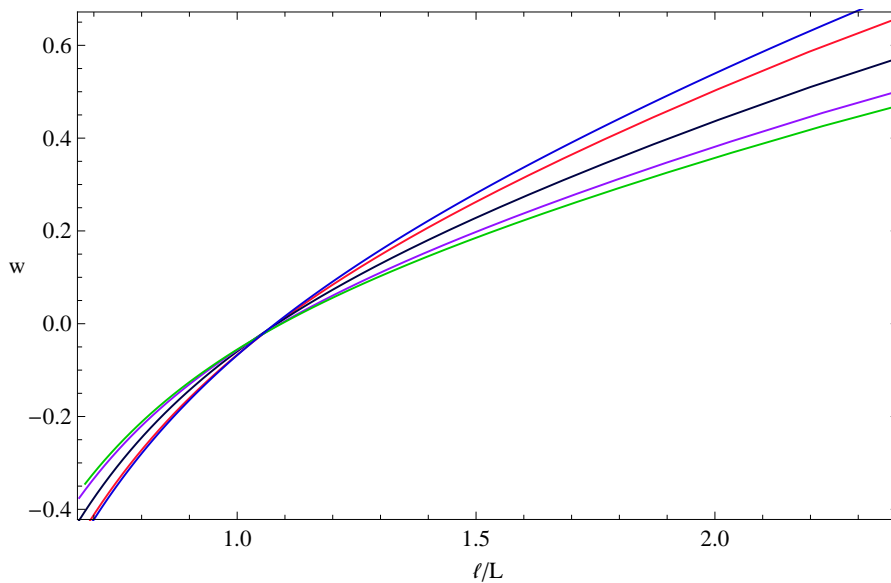


Figure 8: The heavy quark potential as a function of distance ℓ in the case $\zeta = 0.2$. In the right part of the plot, lines from the top to down are for $\mu \leq \mu_c$ (blue), $\mu \simeq 2.134$ (red), $\mu \simeq 3.025$ (black), $\mu \simeq 4.920$ (purple) and $\mu \simeq 5.655$ (green), respectively.

The integrand can be regarded as a Lagrangian and σ as time. Taking advantage of the fact that the Hamiltonian is conserved, we can deduce the equation of motion

$$\frac{dr}{d\sigma} = \pm \frac{r^2 \sqrt{g(r)}}{L} \sqrt{\frac{r^4 f(r)}{r_*^4 f(r_*)} - 1}, \quad (22)$$

where we have used the condition that the geometry is smooth at $r(x=0) = r_*$, i.e., $dr/d\sigma|_{r=r_*} = 0$. Substituting (22) to (21), we obtain the on-shell world sheet action in the connected case

$$S_{x-t}^{con} = \frac{2T}{2\pi\alpha'} \int_{r_*}^{\frac{1}{\epsilon}} dr \sqrt{\frac{f(r)}{g(r)}} \frac{L}{1 - \sqrt{\frac{r^4 f(r)}{r_*^4 f(r_*)}}} = \frac{2TL}{2\pi\alpha'} \left(\frac{1}{\epsilon} + w^{con}\right), \quad (23)$$

where the UV cutoff ϵ has been taken into consideration and w^{con} is a finite part. The distance ℓ is related to r_* by

$$\frac{\ell}{2} = \int_{r_*}^{\frac{1}{\epsilon}} dr \frac{1}{r^2 \sqrt{g(r)}} \frac{L}{\sqrt{\frac{r^4 f(r)}{r_*^4 f(r_*)} - 1}}. \quad (24)$$

For the disconnected configuration, with using the gauge $\tau = t$ and $\sigma = r$ and $x'(r) = 0$, we obtain the regularized on-shell world sheet action as follows.

$$S_{x-t}^{discon} = \frac{2T}{2\pi\alpha'} \int_{r_0}^{\frac{1}{\epsilon}} dr L \sqrt{\frac{f(r)}{g(r)}} = \frac{2TL}{2\pi\alpha'} \left(\frac{1}{\epsilon} + w^{discon} \right). \quad (25)$$

One can see that S_{x-t}^{con} and S_{x-t}^{discon} have the same UV behavior. The divergence in (25) just manifests the infinite mass of heavy quarks. The divergence in (23) can be subtracted by considering the infinite mass of quarks in (25). And thus we can obtain the heavy quark potential $w \equiv w^{con} - w^{discon}$ as a function of the distance ℓ . We find that the behavior of the heavy quark potential is quite similar for different parameters, i.e., β , ζ and μ . We present Figure (8) with $\zeta = 0.2$ as a concrete example. One can see from the figure that in all cases, the heavy quark potential goes roughly linear with the distance in large ℓ region, which implies the dual field theory is a confinement phase, while in the small ℓ region, the potential shows a Coulomb potential behavior, which means that the dual field theory is in a deconfinement phase in the small ℓ region. There is an associated confinement/deconfinement phase transition when one changes the distance ℓ . This feature is consistent with the one shown in Figure (3) through the entanglement entropy calculation. Here the confinement/deconfinement transition point can be identified with the point where the potential vanishes.

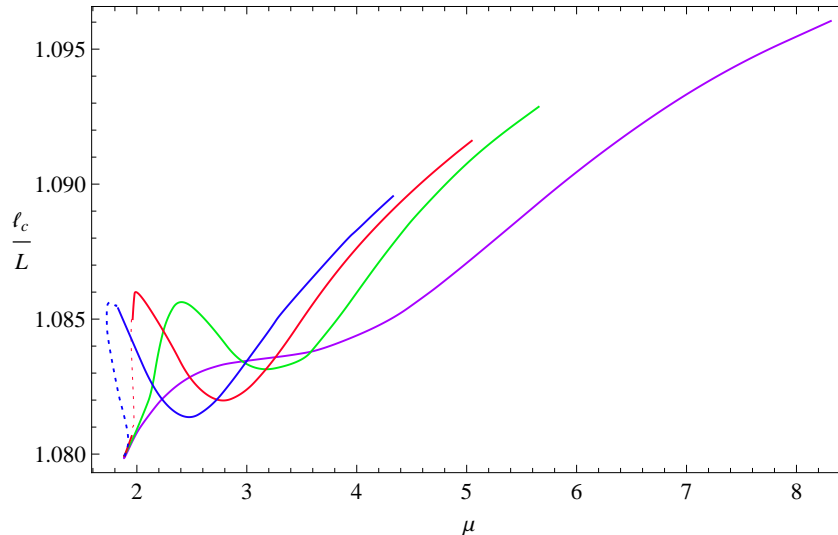


Figure 9: The critical distance ℓ_c as a function of chemical potential. Lines from right to left are for $\zeta = 0$ (purple), $\zeta = 0.2$ (green), $\zeta = 0.65$ (red) and $\zeta = 1.6$ (blue), respectively. The dotted part of the lines for $\zeta = 0.65$ (red) and $\zeta = 1.6$ (blue) are not thermodynamically favored, trace the physical curves by always choosing the solid lines.

In Figure (9) we plot the relation of the critical distance ℓ_c with respect to chemical potential. One can see that ℓ_c increases monotonically when ζ is very small, then a peak

emerges and the position of the peak moves to the left as we increase ζ , finally, the peak is cut off for very large ζ because there is a jump at μ_c for the first order phase transition. One interesting point is that the critical distance is not always a monotonic function of chemical potential. We think that this arises due to the different behavior of the heavy quark potential in the small and large ℓ regions. In Figure (10), we plot the heavy quark potentials versus chemical potential in the deconfinement phase and confinement phase, respectively. We can see clearly that the behavior of the heavy quark potential is quite different in two cases.

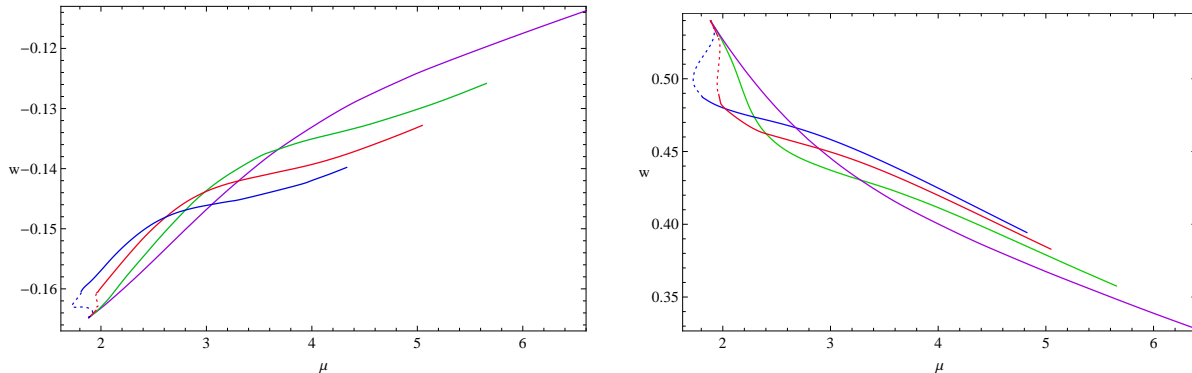


Figure 10: The heavy quark potential as a function of chemical potential at fixed $\ell/L = 0.9$ (left plot) and $\ell/L = 2$ (right plot). Lines are for $\zeta = 0$ (purple), $\zeta = 0.2$ (green), $\zeta = 0.65$ (red) and $\zeta = 1.6$ (blue), respectively. The dotted part of the lines for $\zeta = 0.65$ (red) and $\zeta = 1.6$ (blue) are not thermodynamically favored, trace the physical curves by always choosing the solid lines.

5.2 Spatial Wilson Loop

In terms of gauge/gravity duality, to calculate the VEV of a spatial Wilson loop, we consider a rectangular loop \mathcal{C} along two spatial directions (x, y) [47][48]. The expectation value of the loop can be obtained by the following AdS/CFT dictionary

$$V_s = \int DX e^{-S_{x-y}}. \quad (26)$$

Here X denotes the series of world sheet fields and S_{x-y} stands for a world sheet action. Again, in the large N limit, the saddle point approximation is valid, and we only need to take the minimum value of the Euclidean action among the saddle points. Given the background (4), we can derive the expectation value of the spatial Wilson loop by using

the Nambu-Goto action for S_{x-y}

$$\begin{aligned} S_{x-y} &= \frac{1}{2\pi\alpha'} \int d^2\eta \sqrt{\text{Det}\chi_{ab}} \\ &= \frac{1}{2\pi\alpha'} \int dx dy \sqrt{r^2(r^2 + \frac{L^2}{r^2} \frac{r'(x)^2}{g(r)}),} \end{aligned} \quad (27)$$

with α' the string tension and χ_{ab} the induced world sheet metric with a, b the indices in the $(\eta^1 = x, \eta^2 = y)$ coordinates on the world sheet. We take one of the spatial direction y goes to infinity. The quark and anti-quark are located at $x = \pm \frac{\ell}{2}$, respectively. As the case with the temporal Wilson loop, in this case, there are also two configurations. For the connected configuration, we can make use of $r' \frac{\partial L}{\partial r'} - L = -r_*^2$ and write down equation of motion for $r'(x)$

$$\frac{r^4}{\sqrt{r^2(r^2 + \frac{L^2}{r^2} \frac{r'(x)^2}{g(r)})}} = r_*^2. \quad (28)$$

Here we have used the following boundary condition $r(x=0) = r_*$, $r'(x=0) = 0$. We put the solution of the equation of motion back to the world sheet action (27) and obtain

$$S_{x-y}^{con} = \frac{2Y}{2\pi\alpha'} \int_{r_*}^{\frac{1}{\epsilon}} dr \frac{L}{\sqrt{g(r)}} \frac{r^2}{r^4 - r_*^4} = \frac{2YL}{2\pi\alpha'} \left(\frac{1}{\epsilon} + w^{con} \right), \quad (29)$$

where Y denotes the separation of quark and antiquark in y direction and the distance ℓ in x direction is given by

$$\frac{\ell}{2} = \int_{r_*}^{\frac{1}{\epsilon}} dr \frac{L}{\sqrt{g(r)}} \frac{r_*^2}{r^2} \frac{1}{r^4 - r_*^4}. \quad (30)$$

Similar to the case for the temporal Wilson loop, we can obtain a finite spatial heavy quark potential (pseudo potential) by subtracting the mass of two heavy quarks. The latter is related to the disconnected configuration. For the disconnected configuration, we take the gauge $\eta^1 = x$ and $\eta^2 = y$ and $x'(r) = 0$, and obtain the on-shell world sheet action

$$S_{x-y}^{discon} = \frac{2Y}{2\pi\alpha'} \int_{r_0}^{\frac{1}{\epsilon}} dr \frac{L}{\sqrt{g(r)}} = \frac{2YL}{2\pi\alpha'} \left(\frac{1}{\epsilon} + w^{discon} \right). \quad (31)$$

We find that the behavior of the pseudo potential $w \equiv w^{con} - w^{discon}$ with respect to ℓ is very similar to the one in the case of temporal Wilson loop. We therefore do not show the behavior of the pseudo potential here. Instead, we plot in Figure (11) the critical distance ℓ_c with respect to chemical potential. Here the critical distance ℓ_c is defined by a vanishing pseudo potential as the case in the temporal Wilson loop. We can see that ℓ_c is non-monotonic and a peak appears even when ζ is vanishing, which is a little bit different from the case in Figure (9). For large chemical potential, the critical distance increases

monotonically. Comparing with Figure (7), we find that the critical strip width ℓ_{crit} from entanglement entropy and the critical distance ℓ_c from the spatial Wilson loop are much qualitatively similar with each other. This is expected since both quantities come from the spatial sector of the background soliton solutions.

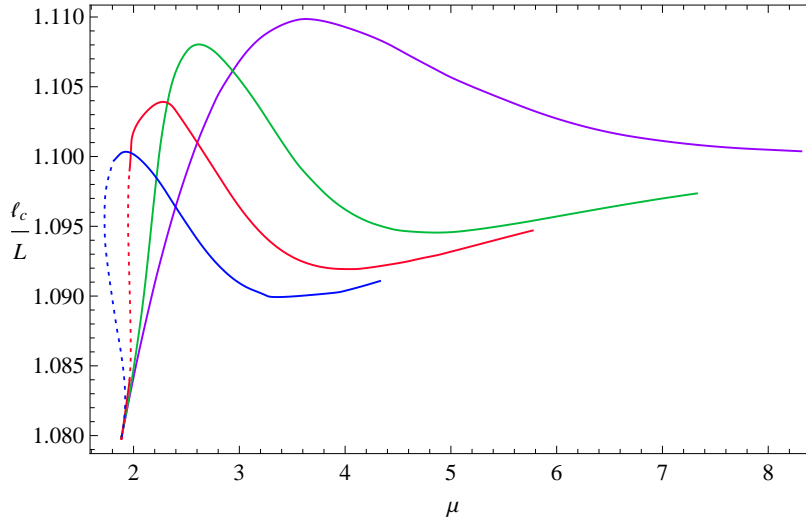


Figure 11: The critical distance ℓ_c as a function of chemical potential in the case of spatial Wilson loop. Lines from right to left are for $\zeta = 0$ (purple), $\zeta = 0.2$ (green), $\zeta = 0.65$ (red) and $\zeta = 1.6$ (blue), respectively. The dotted part of the lines for $\zeta = 0.65$ (red) and $\zeta = 1.6$ (blue) are not thermodynamically favored, trace the physical curves by always choosing the solid lines. Note that the curve for $\zeta = 0$ (purple) will continue to increase for sufficiently large chemical potential as other curves.

But we find that the behavior of the pseudo potential with the change of chemical potential is different from the case in the temporal Wilson loop. In Figure (12) we plot the pseudo potentials with respect to chemical potential for fixed distance $\ell/L = 0.9$ (in the deconfinement phase) and $\ell/L = 2$ (in the confinement phase). In the case of $\ell/L = 0.9$, we see that as ζ is not very large, the behavior of heavy quark potential is qualitatively similar to each other, no matter the order of the phase transition. At the beginning of the phase transition, it firstly decrease in the superconducting phase and then increases continuously for large chemical potential. The position of the bottom moves to small chemical potential side with the increase of ζ . For sufficient large ζ , the bottom is cut off and the pseudo potential increases monotonically with the increase of the chemical potential.

6 Conclusion and Discussions

To better understand the properties of holographic superconductor, we investigated the behaviors of two non-local physical quantities, i.e., entanglement entropy and Wilson loop in the Stückelberg holographic insulator/superconductor model. The model exhibits rich

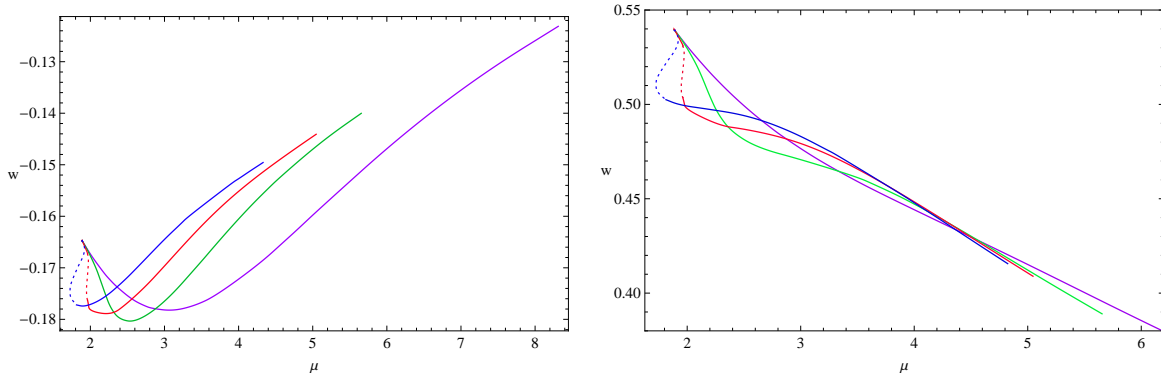


Figure 12: The pseudo potential as a function of chemical potential at fixed $\ell/L = 0.9$ (left plot) and $\ell/L = 2$ (right plot). Lines are for $\zeta = 0$ (purple), $\zeta = 0.2$ (green), $\zeta = 0.65$ (red) and $\zeta = 1.6$ (blue), respectively. The dotted part of the lines for $\zeta = 0.65$ (red) and $\zeta = 1.6$ (blue) are not thermodynamically favored, trace the physical curves by always choosing the solid lines.

phase structure. For small ζ , the transition at μ_c is second order and no discontinuity within the superconducting phase. For intermediate ζ , there is an additional complication. As we can see from the left plot of Figure (2), the grand potential as a function of chemical potential develops a “swallow tail” at a certain chemical potential μ_0 in the superconducting phase. Thus, there is a jump in the condensate within the superconducting phase. For large ζ , the superconducting phase transition becomes first order.

We calculated the entanglement entropy for a strip geometry and the VEV for temporal Wilson loop and spatial Wilson loop in the insulator/superconductor phase transition. Both show that there exists a confinement/deconfinement phase transition (see Figure (3) and Figure (8)). In both cases, we found that the critical width for the strip and the critical distance between quark and antiquark are non-monotonic functions of chemical potential (see Figure (7) and Figure (9)).

There is either a discontinuity of the entanglement entropy or its slope with respect to chemical potential at μ_c , namely, at the insulator/superconductor transition point, which indicates some kind of significant reorganization of the degrees of freedom as new degrees of freedom are expected to emerge in the superconducting phase. These discontinuities of the entanglement entropy or its slope correctly indicate the order of associated phase transition. Beyond the critical chemical potential, we found that the entanglement entropy is not monotonic in the superconducting phase: at the beginning of the transition, the entropy increases and reaches its maximum at a certain chemical potential μ_{max} and then decreases monotonically. This behavior is universal in the holographic insulator/superconductor model. As one increases the model parameter ζ , but keeps the parameter β , the position of the peak μ_{max} moves to the small chemical potential side.

Compared to the phenomenon observed in the entanglement entropy, the (pseudo) heavy quark potential with respect to chemical potential in superconducting phase presents more rich behaviors. For a fixed chemical potential, the heavy quark potential always

increases with the distance between the quark-antiquark pair (see Figure (8)). In the small ℓ region the potential has a Coulomb potential form, while in the large ℓ region, the potential shows a confining potential form, as it is expected. But the behaviors of the heavy quark potential with respect to chemical potential are just opposite to each other in the small ℓ region and in the large ℓ region.

In the spatial Wilson loop case, the pseudo potential shows a non-monotonic behavior with respect to chemical potential in the small ℓ region, but not in the large ℓ region (see Figure (12)). The non-monotonic behavior might be related to the one in the entanglement entropy.

In this paper, we just reported the behaviors of the entanglement entropy and heavy quark potential in the holographic Stückelberg insulator/superconductor model. Unfortunately, due to the lack of the knowledge of the dual field theory in the “bottom-up” approach, we can not completely understand some implications of the behaviors of entanglement entropy and heavy quark potential, in particular, for the non-monotonic behavior, although we tried to give some discussions for this in Ref. [34]. But anyway, different from some physical quantities, such as condensate and charge density, in superconducting phase, we can see that there are various phase structures in superconducting phase by investigating the behaviors of entanglement entropy and Wilson loop. It turns out that these two non-local physical quantities are good probes to study the properties of the holographic phase transition.

In this paper we limited ourselves to the case with $\mathcal{F}(\psi) = \psi^2 + \zeta\psi^6$. For other form of the function, see, for example, Refs.[36, 38, 39], we expect that the result will be qualitatively same. But it is interesting to confirm this. In addition, It would be of great interest to investigate the behavior of entanglement entropy in the holographic p-wave insulator/superconductor case, in order to see whether the non-monotonic behavior is more universal or not.

Acknowledgements

We thank T. Takayanagi for helpful correspondences and in particular for his suggestion to calculate the heavy quark potential in the holographic insulator/superconductor phase transition. This work was supported in part by the National Natural Science Foundation of China (No.10821504, No.10975168, No.11035008 and No.11205226), and in part by the Ministry of Science and Technology of China under Grant No. 2010CB833004. SH and LFL would like appreciate the general financial support from China Postdoctoral Science Foundation No. 2012M510562 and No. 2012M510563 respectively. SH also would like thank for Department of Electrophysics of National Chiao-Tung University, National Taiwan university and the ”International School On Strings And Fundamental Physics” held at Hamburg, for their hospitality and financial support. The authors are grateful to Zhang-Yu Nie, Wen-Yu Wen, Yi Yang, Hai-Qing Zhang and Yun-Long Zhang for useful discussions.

References

- [1] Ryu, S., Hatsugai, Y. “Entanglement entropy and the Berry phase in the solid state,” *Phys. Rev. B* **73**, 245115 (2006) [arXiv:cond-mat/0601237].
- [2] L. Amico, R. Fazio, A. Osterloh and V. Vedral, “Entanglement in many-body systems,” *Rev. Mod. Phys.* **80**, 517 (2008) [quant-ph/0703044 [QUANT-PH]].
- [3] J. M. Maldacena, “The large N limit of superconformal field theories and supergravity,” *Adv. Theor. Math. Phys.* **2**, 231 (1998) [*Int. J. Theor. Phys.* **38**, 1113 (1999)] [arXiv:hep-th/9711200].
- [4] S. S. Gubser, I. R. Klebanov and A. M. Polyakov, “Gauge theory correlators from non-critical string theory,” *Phys. Lett. B* **428**, 105 (1998) [arXiv:hep-th/9802109].
- [5] E. Witten, “Anti-de Sitter space and holography,” *Adv. Theor. Math. Phys.* **2**, 253 (1998) [arXiv:hep-th/9802150].
- [6] O. Aharony, S. S. Gubser, J. M. Maldacena, H. Ooguri and Y. Oz, *Phys. Rept.* **323**, 183 (2000) [arXiv:hep-th/9905111].
- [7] S. Ryu and T. Takayanagi, “Holographic derivation of entanglement entropy from AdS/CFT,” *Phys. Rev. Lett.* **96**, 181602 (2006) [hep-th/0603001].
- [8] T. Nishioka, S. Ryu and T. Takayanagi, “Holographic Entanglement Entropy: An Overview,” *J. Phys. A* **42**, 504008 (2009) [arXiv:0905.0932 [hep-th]].
- [9] T. Takayanagi, “Entanglement Entropy from a Holographic Viewpoint,” arXiv:1204.2450 [gr-qc].
- [10] S. A. Hartnoll, C. P. Herzog and G. T. Horowitz, “Building a Holographic Superconductor,” *Phys. Rev. Lett.* **101**, 031601 (2008) [arXiv:0803.3295 [hep-th]].
- [11] T. Albash and C. V. Johnson, “A Holographic Superconductor in an External Magnetic Field,” *JHEP* **0809**, 121 (2008) [arXiv:0804.3466 [hep-th]].
- [12] R. -G. Cai, L. Li, H. -Q. Zhang and Y. -L. Zhang, “Magnetic Field Effect on the Phase Transition in AdS Soliton Spacetime,” *Phys. Rev. D* **84**, 126008 (2011) [arXiv:1109.5885 [hep-th]].
- [13] G. T. Horowitz and M. M. Roberts, “Holographic Superconductors with Various Condensates,” *Phys. Rev. D* **78**, 126008 (2008) [arXiv:0810.1077 [hep-th]].
- [14] E. J. Brynjolfsson, U. H. Danielsson, L. Thorlacius and T. Zingg, “Holographic Superconductors with Lifshitz Scaling,” *J. Phys. A* **43**, 065401 (2010) [arXiv:0908.2611 [hep-th]].
- [15] R. -G. Cai and H. -Q. Zhang, “Holographic Superconductors with Horava-Lifshitz Black Holes,” *Phys. Rev. D* **81**, 066003 (2010) [arXiv:0911.4867 [hep-th]].
- [16] G. T. Horowitz and M. M. Roberts, “Zero Temperature Limit of Holographic Superconductors,” *JHEP* **0911**, 015 (2009) [arXiv:0908.3677 [hep-th]].
- [17] G. T. Horowitz, J. E. Santos and B. Way, “A Holographic Josephson Junction,” *Phys. Rev. Lett.* **106**, 221601 (2011) [arXiv:1101.3326 [hep-th]].

- [18] Y. -Q. Wang, Y. -X. Liu, R. -G. Cai, S. Takeuchi and H. -Q. Zhang, “Holographic SIS Josephson Junction,” arXiv:1205.4406 [hep-th].
- [19] M. Montull, O. Pujolas, A. Salvio and P. J. Silva, “Flux Periodicities and Quantum Hair on Holographic Superconductors,” Phys. Rev. Lett. **107**, 181601 (2011) [arXiv:1105.5392 [hep-th]].
- [20] N. Bobev, A. Kundu, K. Pilch and N. P. Warner, “Minimal Holographic Superconductors from Maximal Supergravity,” JHEP **1203**, 064 (2012) [arXiv:1110.3454 [hep-th]].
- [21] Y. Liu, Y. Peng and B. Wang, “Gauss-Bonnet holographic superconductors in Born-Infeld electrodynamics with backreactions,” arXiv:1202.3586 [hep-th].
- [22] J. Erdmenger, P. Kerner and H. Zeller, “Transport in Anisotropic Superfluids: A Holographic Description,” JHEP **1201**, 059 (2012) [arXiv:1110.0007 [hep-th]].
- [23] S. S. Gubser and S. S. Pufu, “The Gravity dual of a p-wave superconductor,” JHEP **0811**, 033 (2008) [arXiv:0805.2960 [hep-th]].
- [24] S. A. Hartnoll and R. Pourhasan, “Entropy balance in holographic superconductors,” JHEP **1207**, 114 (2012) [arXiv:1205.1536 [hep-th]].
- [25] J. Erdmenger, P. Kerner and S. Muller, “Towards a Holographic Realization of Homes’ Law,” arXiv:1206.5305 [hep-th].
- [26] M. Montull, O. Pujolas, A. Salvio and P. J. Silva, “Magnetic Response in the Holographic Insulator/Superconductor Transition,” JHEP **1204**, 135 (2012) [arXiv:1202.0006 [hep-th]].
- [27] L. Barclay, R. Gregory, S. Kanno and P. Sutcliffe, “Gauss-Bonnet Holographic Superconductors,” JHEP **1012**, 029 (2010) [arXiv:1009.1991 [hep-th]].
- [28] R. -G. Cai, Z. -Y. Nie and H. -Q. Zhang, “Holographic p-wave superconductors from Gauss-Bonnet gravity,” Phys. Rev. D **82**, 066007 (2010) [arXiv:1007.3321 [hep-th]].
- [29] M. Siani, “Holographic Superconductors and Higher Curvature Corrections,” JHEP **1012**, 035 (2010) [arXiv:1010.0700 [hep-th]].
- [30] R. -G. Cai, Z. -Y. Nie and H. -Q. Zhang, “Holographic Phase Transitions of P-wave Superconductors in Gauss-Bonnet Gravity with Back-reaction,” Phys. Rev. D **83**, 066013 (2011) [arXiv:1012.5559 [hep-th]].
- [31] J. -P. Wu, Y. Cao, X. -M. Kuang and W. -J. Li, “The 3+1 holographic superconductor with Weyl corrections,” Phys. Lett. B **697**, 153 (2011) [arXiv:1010.1929 [hep-th]].
- [32] T. Albash and C. V. Johnson, “Holographic Studies of Entanglement Entropy in Superconductors,” JHEP **1205**, 079 (2012) [arXiv:1202.2605 [hep-th]].
- [33] R. -G. Cai, S. He, L. Li and Y. -L. Zhang, “Holographic Entanglement Entropy on P-wave Superconductor Phase Transition,” JHEP **1207**, 027 (2012) [arXiv:1204.5962 [hep-th]].
- [34] R. -G. Cai, S. He, L. Li and Y. -L. Zhang, “Holographic Entanglement Entropy in Insulator/Superconductor Transition,” JHEP **1207**, 088 (2012) [arXiv:1203.6620 [hep-th]].

- [35] T. Nishioka, S. Ryu and T. Takayanagi, “Holographic Superconductor/Insulator Transition at Zero Temperature,” *JHEP* **1003**, 131 (2010) [arXiv:0911.0962 [hep-th]].
- [36] S. Franco, A. Garcia-Garcia and D. Rodriguez-Gomez, “A General class of holographic superconductors,” *JHEP* **1004**, 092 (2010) [arXiv:0906.1214 [hep-th]].
- [37] G. T. Horowitz and B. Way, “Complete Phase Diagrams for a Holographic Superconductor/Insulator System,” *JHEP* **1011**, 011 (2010) [arXiv:1007.3714 [hep-th]].
- [38] F. Aprile and J. G. Russo, “Models of Holographic superconductivity,” *Phys. Rev. D* **81**, 026009 (2010) [arXiv:0912.0480 [hep-th]].
- [39] Y. Peng, Q. Pan and B. Wang, “Various types of phase transitions in the AdS soliton background,” *Phys. Lett. B* **699**, 383 (2011) [arXiv:1104.2478 [hep-th]].
- [40] T. Nishioka and T. Takayanagi, “AdS Bubbles, Entropy and Closed String Tachyons,” *JHEP* **0701**, 090 (2007) [hep-th/0611035].
- [41] I. R. Klebanov, D. Kutasov and A. Murugan, “Entanglement as a probe of confinement,” *Nucl. Phys. B* **796**, 274 (2008) [arXiv:0709.2140 [hep-th]].
- [42] R. C. Myers and A. Singh, “Comments on Holographic Entanglement Entropy and RG Flows,” *JHEP* **1204**, 122 (2012) [arXiv:1202.2068 [hep-th]].
- [43] J. M. Maldacena, “Wilson loops in large N field theories,” *Phys. Rev. Lett.* **80**, 4859 (1998) [arXiv:hep-th/9803002].
- [44] S. J. Rey, S. Theisen and J. T. Yee, “Wilson-Polyakov loop at finite temperature in large N gauge theory and anti-de Sitter supergravity,” *Nucl. Phys. B* **527**, 171 (1998) [arXiv:hep-th/9803135].
- [45] A. M. Polyakov, “String theory and quark confinement,” *Nucl. Phys. Proc. Suppl.* **68**, 1 (1998) [arXiv:hep-th/9711002].
- [46] R. -G. Cai, S. He and D. Li, “A hQCD model and its phase diagram in Einstein-Maxwell-Dilaton system,” *JHEP* **1203**, 033 (2012) [arXiv:1201.0820 [hep-th]].
- [47] O. Andreev and V. I. Zakharov, “The Spatial String Tension, Thermal Phase Transition, and AdS/QCD,” *Phys. Lett. B* **645**, 437 (2007) [arXiv:hep-ph/0607026]; O. Andreev, “The Spatial String Tension in the Deconfined Phase of SU(N) Gauge Theory and Gauge/String Duality,” *Phys. Lett. B* **659**, 416 (2008) [arXiv:0709.4395 [hep-ph]].
- [48] D. Li, S. He, M. Huang and Q. -S. Yan, “Thermodynamics of deformed AdS₅ model with a positive/negative quadratic correction in graviton-dilaton system,” *JHEP* **1109**, 041 (2011) [arXiv:1103.5389 [hep-th]].